SURFACE CHARACTERIZATION AND OPTICAL NAVIGATION AT THE ROSETTA FLYBY OF ASTEROID LUTETIA

R. Pardo de Santayana [(1)], M. Lauer [(2)], P. Muñoz [(3)], and F. Castellini [(4)]
[(1)] *GMV located at ESOC, ramon.pardo@esa.int*
[(2)] *ESA/ ESOC, mathias.lauer@esa.int*
[(3)] *GMV located at ESOC, pablo.munoz@esa.int*
[(4)] Telespazio-*Vega located at ESOC, francesco.castellini@esa.int*

Abstract: *The ESA interplanetary spacecraft (S/C) Rosetta was launched in March 2004 to rendezvous with comet 67P/ Churyumov-Gerasimenko ten years later in 2014. In July 2010 the S/C flew by asteroid Lutetia. During the flyby, high-resolution images of the asteroid were taken by the on-board science camera and were processed to reconstruct the flyby geometry and a coarse shape model. This paper presents an improvement in the optical navigation and shape reconstruction using landmark maps. This technique was developed in the frame of the Rosetta cometary phase with the intention to be applied during the near-comet navigation.*
Keywords: *Optical Navigation, Shape Reconstruction, Photoclinometry, Photogrammetry*.

1. Introduction

The ESA interplanetary spacecraft (S/C) Rosetta was launched in March 2004 to rendezvous with comet 67P/ Churyumov-Gerasimenko ten years later in 2014. The overall trajectory contained several planetary swing-bys (Earth and Mars) and two asteroid flybys (Steins in 2008 and Lutetia in 2010).

During the Lutetia flyby in July 2010, the onboard instrument OSIRIS NAC (Narrow Angle Camera, [1]) obtained high-resolution images of the asteroid. An overview of the optical data processing for navigation was presented at the ISSFD2012 [2], were pixel positions of landmarks were manually determined using a graphical user interface.

This paper presents an improvement in the optical navigation and shape reconstruction using landmark maps (L-maps). This procedure for identifying landmarks was first developed by R. W. Gaskell [5] [8]. However, the work presented here, details an implementation with a technique that combines stereophotoclinometry and stereophotogrammetry.

This technique is applied to the Lutetia scenario. L-maps were generated all around the observed surface of the asteroid, and automatic landmark observations were obtained for all the available images acquired within a certain distance from Lutetia. The spacecraft relative position and attitude as well as the comet-fixed landmarks grid were reconstructed with two different estimation methods. The first, known as “bundle adjustment”, is based on purely optical information, whereas the second also includes radiometric data and dynamic information in the full orbit determination solution.

The L-maps were combined to assemble a medium-resolution shape model which represents a significantly better characterization of Lutetia with respect to the previous method that involved a silhouette carving technique (ISSFD2012). The shape recovery’s accuracy is assessed with the support of image simulation software. Synthetic images have been rendered using the shape of the asteroid and the reconstructed flyby geometry to be compared against the real pictures.

The L-maps technique was developed in the frame of the Rosetta cometary-phase preparation activities as part of the optical navigation framework which will be used for near-comet operations. A broad overview of the optical navigation operational concept and of the main techniques developed for this purpose was given in [3]. The baseline methodology described there foresees a manual processing through a GUI to obtain landmark measurements for navigation and comet characterization. This method was selected for its robustness in view of the totally unknown comet environment and possibly changing surface features. However it is intended to gradually phase the L-maps technique in the operations during the long comet-phase, in order to drastically relieve the operational workload, as well as to increase the landmark coverage of Churyumov-Gerasimenko and to improve the quality of the optical measurements.

2. Theoretical background and implementation

L-maps are small digital elevation maps (DEM) centred in particular surface features, landmarks. These three dimensional surfaces can be rendered to obtain the simulated visual appearance of landmarks under different viewing angles and different sun incidences.

As a first step, a set of L-maps are reconstructed from images where the relative geometry is known. This will be possible if the landmarks are visible several times with different illumination and observation conditions. Finally, the simulated visual appearance of landmarks is predicted and correlated with actual images to generate landmark observations. The robustness of this technique lies on the fact that landmarks can be identified over a wide range of illumination and observation conditions. However its performance decreases in extreme cases such as very low phase angles, high emission angles or high incidence angles [4].

2.1. Photometry

The reflectance of a surface is defined by three angles: incidence angle, i, which is the angle between Sun incidence, $\bar{i}$, and surface normal, $\bar{n}$; emission angle, e, which is the angle between emission, $\bar{e}$, and surface normal; and phase angle, α, which is the angle between Sun incidence and emission.

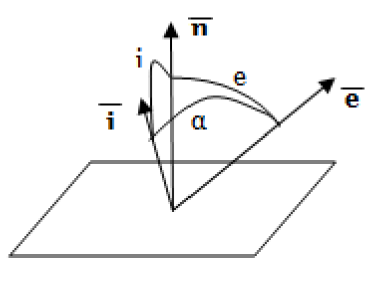

Figure 1. Angle definitions in photometry.

The raw signal S in Digital Units [DU], which is recorded on a CCD pixel, is modelled as:

$$S = \Lambda(t_I, K_{CAM}, d_S) \cdot a \cdot R(\alpha, i, e) + \Phi$$

$$\Lambda = K_0 \cdot \frac{t_I \cdot K_{CAM}}{d_S}$$

$$R(\alpha,i,e) = P(\alpha) \cdot [(1 - L(\alpha)) \cdot R_L(i) + L(\alpha) \cdot R_{LS}(i,e)]$$

$$R_L(i) = Cos(i) = \bar{n} \cdot \bar{i}$$

$$R_{LS}(i,e) = \frac{Cos(i)}{Cos(i) + Cos(e)} = \frac{\bar{n} \cdot \bar{i}}{\bar{n} \cdot (\bar{i} + \bar{e})}$$

$$L(\alpha) = e^{-\frac{\alpha}{\alpha_0}}$$

$$P(\alpha) = e^{-\frac{\alpha}{\beta_0}}$$

Where Λ is a function of the sun distance d_S, the camera conversion factor K_{CAM} (i.e. converting from the physical intensity of the incoming flux on a CCD pixel in [W/m^2/sr] to the pixel's signal rate in [DU/s]) and the integration time t_I; a is the surface albedo; R is the reflectance function formed of a linear combination of Lambert reflectance, $R_{L,}$ and Lommel-Seeliger reflectance, R_{LS}; L is the McEwen Lunar function; P is a phase function; and Φ is the CCD background level.

This model requires of the estimation of three parameters (K_0, α_0 and β_0). α_0 is a characteristic angle that represents a gradual transition from Lommel-Seeliger reflectance to Lambert reflectance. The Lommel-Seeliger term models specular reflection effects and the Lambert term models pure diffuse reflection. β_0 is a scale angle that models an exponential decrease of the reflectance with the phase angle. It may be required to implement a polynomial phase function if it was found that the real phase function differs substantially from an exponential function. K_0 is a constant scale factor which includes the sun emitting power and is combined with the sun distance, integration time, sun distance and camera gain to transform the non-dimensional reflectance function first into physical units [W/m^2/sr] and then into DU/s and DU. .

2.2. L-Map reconstruction

An L-map is defined by a landmark position, an L-map reference frame, the cell number, the cell size and a height and albedo map. The cells are aligned with the X and Y axes with a height associated to them representing surface points along the Z axis and over the XY plane. The landmark is located at the central cell. The cell size is selected such that it corresponds approximately to a pixel transversal projection at the distance in which the images are being acquired.

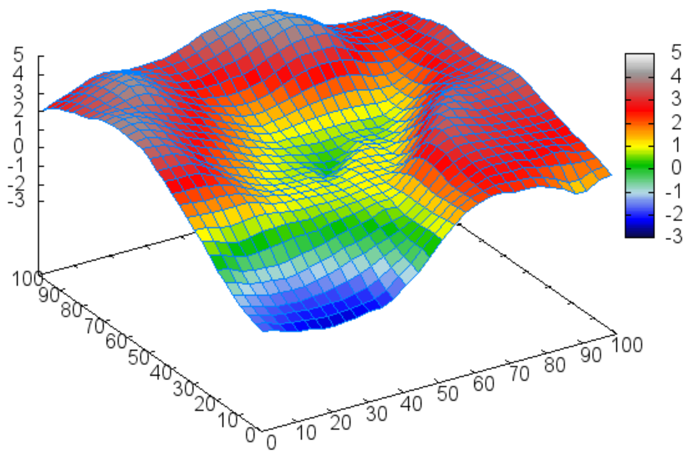

Figure 2. Digital elevation map (DEM) of a landmark in asteroid Lutetia. The height in kilometers is shown per cell.

In this section, the steps involved in the algorithm to reconstruct a digital elevation map from a set of images are described.

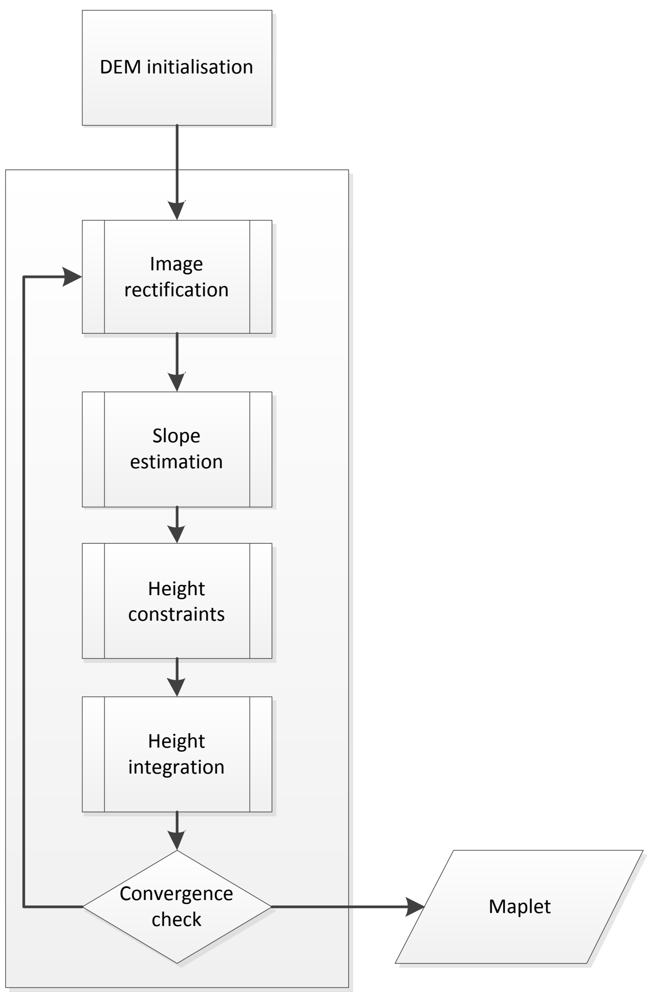

Figure 3. DEM generation diagramm.

2.2.1. DEM initialisation

An L-map is initialised with a landmark position in body frame. This landmark position becomes the origin of the L-map reference frame. The Z axis is aligned initially with the landmark position vector. The X axis points to the East and the Y axis to the North:

$$\bar{u}_z = \frac{\overline{lm}}{\left\|\overline{lm}\right\|}$$

$$\bar{u}_x = \frac{\bar{k} \times \bar{u}_z}{\left\|\bar{k} \times \bar{u}_z\right\|}$$

$$\bar{u}_y = \bar{u}_z \times \bar{u}_x$$

All heights and slopes are set to zero. This approximation assumes a flat surface normal to the landmark vector in case the topography is completely unknown. In general however, the surface is known with some degree of accuracy and a given DEM or a shape model can be used to initialise the heights and slopes. The landmark position used to start this process has to be estimated with an uncertainty comparable or smaller than the cell size.

2.2.2. Image rectification

The relative geometry is assumed known. That means that the camera position and orientation in body fixed frame are given. Additionally, an estimation of the L-map local heights is provided. Therefore each image, in which the landmark is visible, can be rectified by mapping signal values to each L-map cell.

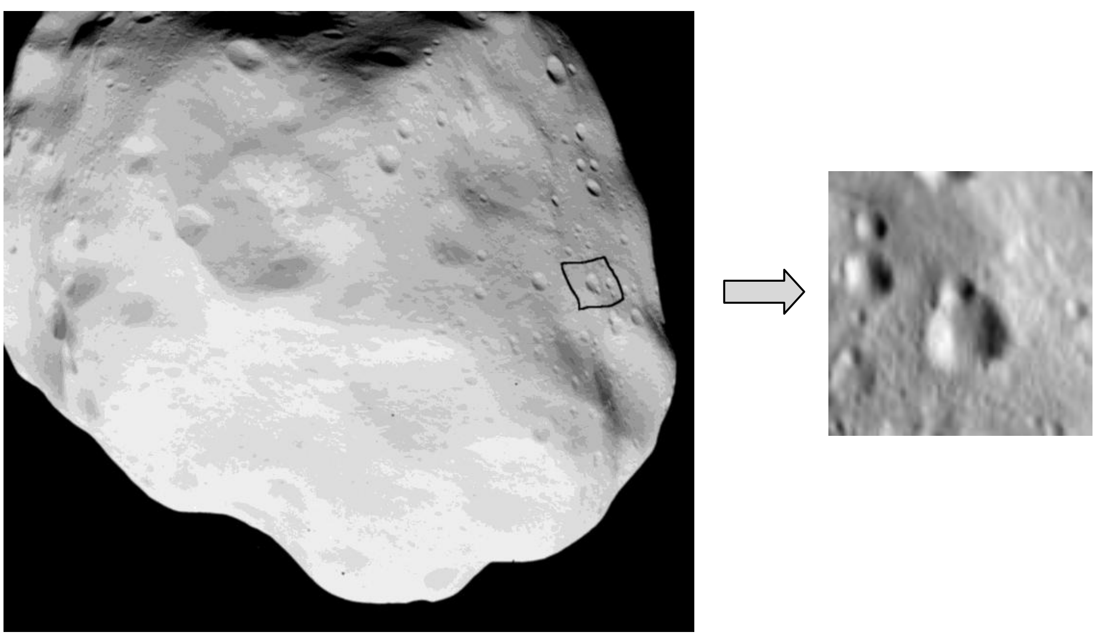

Figure 4. Image rectification example from asteroid Lutetia.

Each L-map cell can be converted into a camera direction:

$$\overline{p_{maplet}}(i,j) = \overline{lm} + \left(i - \frac{(n+1)}{2}\right)\cdot\overline{u_x} + \left(j - \frac{(n+1)}{2}\right)\cdot\overline{u_y} + h(i,j)\cdot\overline{u_z}$$

$$\overline{p_{CAM}}(i,j) = A_{CAM}\cdot(\overline{p_{maplet}}(i,j) - \overline{sc})$$

$$\overline{d} = \frac{\overline{p_{CAM}}}{\left\|\overline{p_{CAM}}\right\|}$$

With the corresponding camera model, the direction can be converted to pixel position and a signal value is read using a bilinear interpolation with the four closest pixels.

The same process is performed with all images complying with certain photometric criteria, namely, emission and incidence angles lower than 60 degrees and phase angles between 5 and 90 degrees. Additionally, images where the cell size is greater than three times the pixel size at that distance or smaller than a third of the pixel size are filtered out.

2.2.3. Slope estimation

The surface normal can be expressed as a function of t_1 and t_2, which are the slopes along X and Y axes respectively:

$$\overline{n} = \frac{(-t_1, -t_2, 1)}{\sqrt{t_1^{\,2} + t_2^{\,2} + 1}}$$

The vector e and i are known, therefore the CCD signal and its derivatives can be expressed as a function of t_1, t_2 and a. Therefore at every L-map cell, the slopes, t_1 and t_2 and the albedo, a, can be estimated given three or more rectified images using a linear least squares method. This technique is known as stereophotoclinometry [5]. And by solving on the cells one by one, full slope maps and albedo map can be obtained.

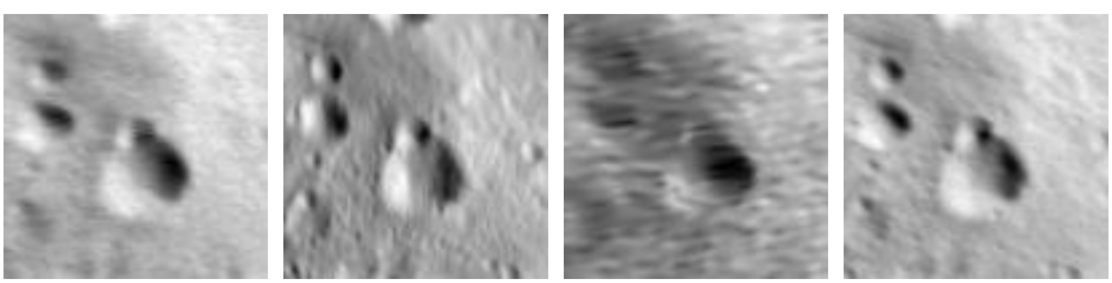

Figure 5. Rectified images from a landmark on asteroid Lutetia.

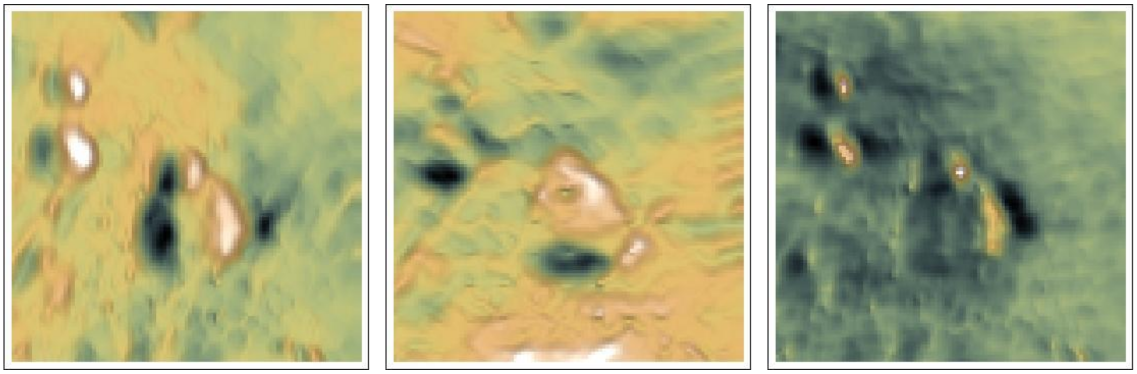

Figure 6. Slopes and albedo map of a landmark on asteroid Lutetia (t_1 left, t_2 centre, albedo right).

A check on dark cells and occulted cells is required prior to the slope estimation process. If a cell is occulted by another in the direction of the sun or the line of sight, the signal that was read from the image is flagged and will be left out of the estimation process.

2.2.4. Height constraints

When integrating heights from slopes there always is a constant of integration to determine, the reference height. Some height values have to be provided to constrain the height map. There are four sources of height values that can be used: the landmarks estimated position, anchor points obtained with stereophotogrammetry, limb projections and shape models. Only the first two methods have been implemented at present but additional sources of height values could be added in the future. The first method consists on projecting the landmarks along the L-map normal onto the XY plane to find out which cell they correspond to. The height is then computed as the distance from the landmark to the XY plane. The second method is more complex. A grid of anchor points is distributed over the L-map surface. Those anchor points are identified in every rectified image and their Cartesian coordinates are estimated. The algorithm is explained below.

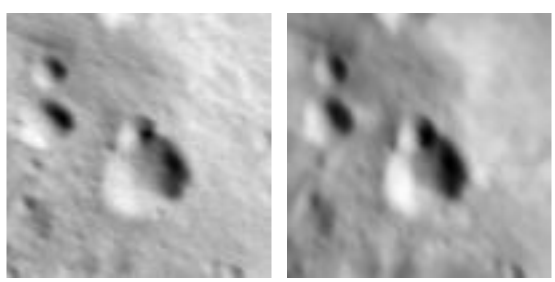

Figure 7. Example of a rectified image (left) and simulated L-map (right) pair.

Since the albedo and slopes are known at this stage, the appearance of the rectified image can be simulated and compared to the rectified image itself. Then, points on the simulated L-map are correlated with the rectified image. This produces observations of local L-map anchor points. With several observations of those local features on different rectified and simulated image pairs;

the anchor point position can be obtained with stereophotogrammetry [6] techniques. Once the anchor point position is known the associated height can be constrained following an analogue process to the “landmark projection” mentioned above. This can be done with a number of anchor points distributed over the body. Experience shows that grids of 7x7, 9x9 or 11x11 are a good choice as a trade of between computation time and performance.

2.2.5. Height integration

The input of this step is a small population of heights over the L-map and two full slope maps and the goal is to obtain a full height map. There are numerous methods with this purpose available in the literature, namely, path integration, Fourier filtering, local integration and direct linear system solving. The latter was the choice due to its performance and fast convergence when using sparse matrix algorithms. The implementation followed the LSQR algorithm [7] to solve the sparse linear system of equations:

$$\frac{h^0{}_{i,j}}{\sigma^h{}_{i,j}} = \frac{h_{i,j}}{\sigma^h{}_{i,j}}$$

$$\frac{t1_{i,j}}{\sigma^{t1}{}_{i,j}} = \frac{h_{i-2,j} - 4 \cdot h_{i-1,j} + 3 \cdot h_{i,j}}{2 \cdot dl \cdot \sigma^{t1}{}_{i,j}}$$

$$\frac{t2_{i,j}}{\sigma^{t2}{}_{i,j}} = \frac{h_{i,j-2} - 4 \cdot h_{i,j-1} + 3 \cdot h_{i,j}}{2 \cdot dl \cdot \sigma^{t2}{}_{i,j}}$$

The slopes are approximated with second order retarded differences scheme for numerical stability reasons. The convergence criterion is established on the height difference from one iteration step to the next. Once the RMS of the height difference is below a certain fraction of the cell size for three consecutive steps the L-map is assumed converged.

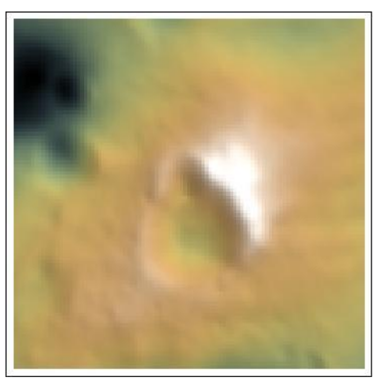

Figure 8. Height map of a landmark on asteroid Lutetia.

2.3. Landmark observation

Once there is a wide L-map coverage of the body, observations of the reconstructed L-maps can be attempted on new images given a good prediction on the observing conditions.

2.3.1. Image matching

It is believed that during operations the main source of error on the relative geometry will be the spacecraft position in body frame. The radial component of this error does not affect our purposes significantly. However the transversal error is of great importance. Therefore, before attempting an L-map observation, it is required to assess and correct (if necessary) this transversal shift.

The options envisaged to correct a transversal shift are: manual limb matching of the body with a dedicated GUI for which a shape model is required; and correlating the expected image with the true image. The later can use L-maps to render the expected image as can be seen below.

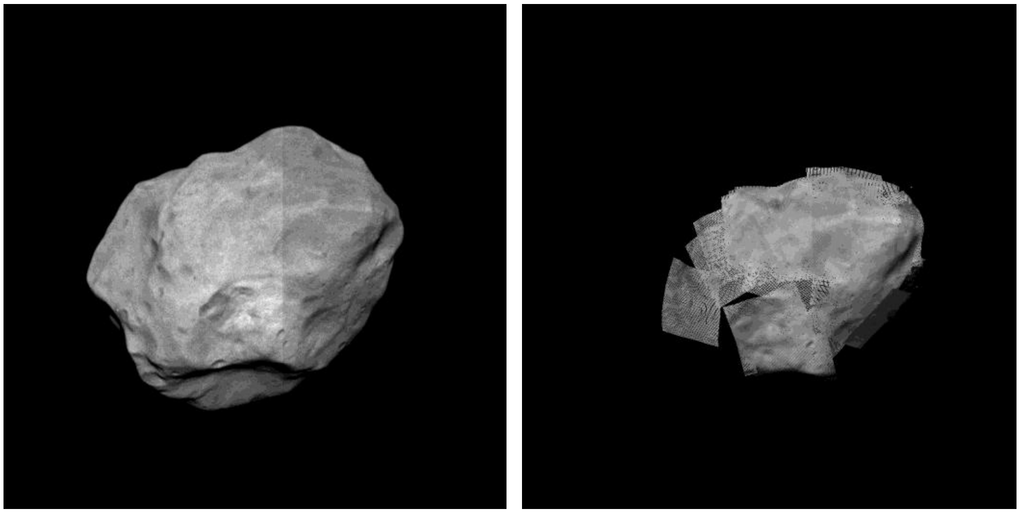

Figure 9. Example of a real image (left) and simulated image (right) pair.

This method simulates all L-maps that comply with a range of incidence, emission and phase angles which are then translated into an image. The matching method is analogous to the L-map matching method explained in the next section in detail.

2.3.2. L-map matching

Once the geometry is estimated with errors on the order of a few pixels, it is possible to generate new landmark observations with the previously reconstructed L-maps. Firstly, the rectified image and the simulated L-map are obtained.

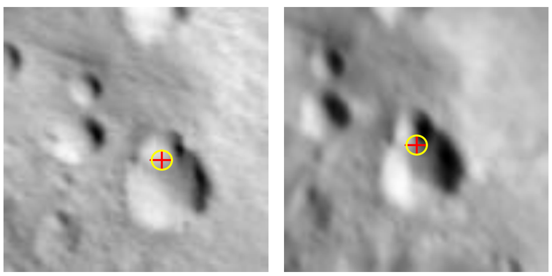

Figure 10. Example of a rectified image (left) and simulated L-map (right) pair with a landmark observation.

Then, the rectified image is shifted along the XY plane to find the maximum correlation. The correlation is defined as:

$$Correlation = \frac{\sum_i \sum_j \left[\left(x_{ij} - \bar{x} \right) \cdot G(r) \right]}{\sqrt{\sum_i \sum_j \left[\left(x_{ij} - \bar{x} \right)^2 \cdot G(r) \right]}} \cdot \frac{\sum_i \sum_j \left[\left(y_{ij} - \bar{y} \right) \cdot G(r) \right]}{\sqrt{\sum_i \sum_j \left[\left(y_{ij} - \bar{y} \right)^2 \cdot G(r) \right]}}$$

$$G(r) = e^{-\frac{r^2}{2 \cdot \sigma^2}}$$

Where i and j are the L-map cell indexes, x is the signal on the rectified image and y the signal of the simulated L-map, G is a Gaussian distribution centred on the L-map centre. r is the distance to the L-map centre in cells and sigma the standard deviation of the Gaussian distribution (around one sixth of the L-map size).

An example of the correlation map between the image pair of Fig.10 is shown in Fig. 11 where an absolute maximum is found with a very high correlation, 0.95. It should be noted that there are local maximums of lower correlation in the vicinity therefore following the gradient might not work if the initial guess is too far.

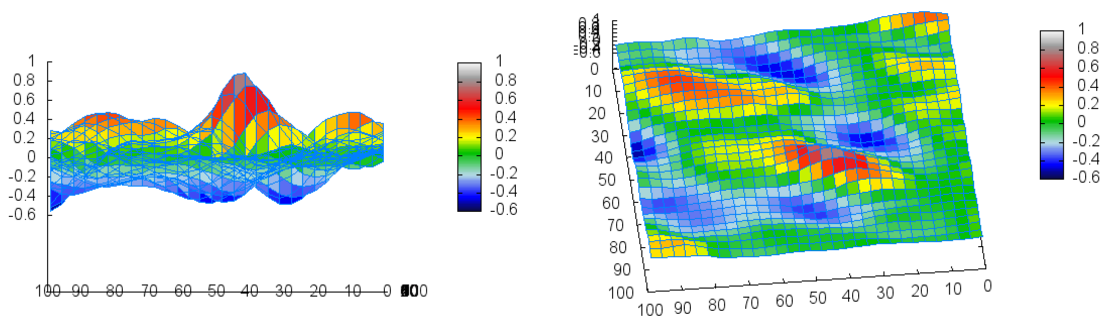

Figure 11 Correlation map between simulated L-map and rectified image as the rectified image shifts along the X and Y axes. Profile view (left) and top view (right)

A match of higher accuracy is achieved by approximating the autocorrelation function with a paraboloid in the proximity of the cell where the highest correlation was found. That is, the maximum correlation is found by second degree interpolation. This way sub-cell accuracy can be obtained on the landmark observation.

The mean curvature of the aforementioned paraboloid relates a shift in the L-map plane with a drop in correlation. By using this relationship, it is possible to compute the uncertainty of the observation. The drop in correlation is 1-MaxCorrelation (correlation drop is 0.05 on Fig.11). The obtained shift in the L-map plane is taken as the 3-sigma value for the uncertainty on the observation.

The observation on the L-map surface is converted into a pixel position on the image as was exposed in section 2.2.2 (image rectification step). The uncertainty of the observation is also converted from cell units to pixel units taking into account the surface tilt and the cell size.

3. Results on the Lutetia flyby

A series of Lutetia images were acquired in situ by Rosetta with the Osiris science camera during the flyby both with the narrow angle camera, NAC, and the wide angle camera, WAC. Due to the high flyby speed of the S/C of ca. 15 km/s, the apparent size of the asteroid was changing considerably between the images. In the first processed image, taken about 50 minutes prior to closest approach, the apparent diameter of the body occupies less than 150 pixels of the NAC. Whereas, at closest approach, the apparent diameter even exceeds the full frame of 2048 by 2048 pixels.

3.1 Landmark observations

The strategy to deal with the apparent size change of a factor of 15 was to generate three separate sets of L-maps with 0.1, 0.3 and 0.5 km of cell size. Each size was selected as the optimum size for a different asteroid distance and therefore covering the entire flyby. In total, 5926 observations were obtained, with a total of 249 different landmarks in 90 images.

At this step, S/C and landmark positions were reconstructed from the optical measurements using a bundle adjustment technique. A detailed description of this process is provided in [8]. This initial reconstruction was not using any kinematic model, but only fitting the geometric positions of the landmarks and the camera to the observations in an arbitrarily scaled frame. The reconstruction consisted in estimating all unknown parameters from the landmark observations. These parameters were the relative position and camera attitude of the S/C (6 parameters per image) and the landmark positions in asteroid frame (3 parameters per landmark).

The bundle adjustment provides a preliminary assessment on the quality of the landmark observations, prior to their use as observables in the orbit determination software. In Fig. 12 the observation residuals are presented in terms of pixels and in Fig.13 in terms of a priori uncertainties. Two conclusions can be derived from the analysis of these results. First, the L-map observations quality is similar over the entire range of distances to the asteroid with both NAC and WAC images. Secondly, the assigned a priori uncertainties are consistent with the residuals. The RMS (residual) is 0.7 pixels in contrast with the 1.5 pixels obtained with manual observations in [2].

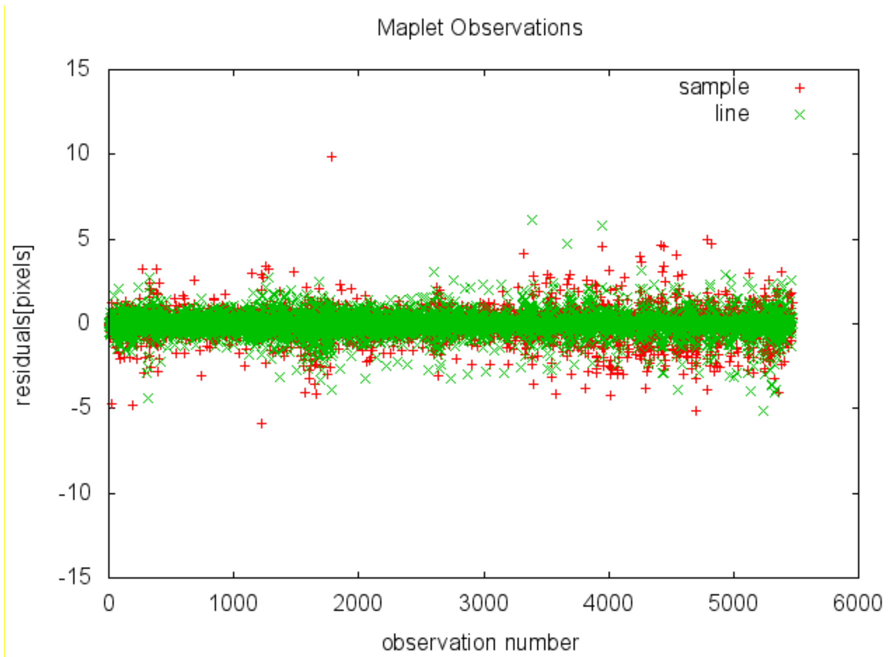

Figure 12. Bundle adjustment residuals in pixels on landmark observations.

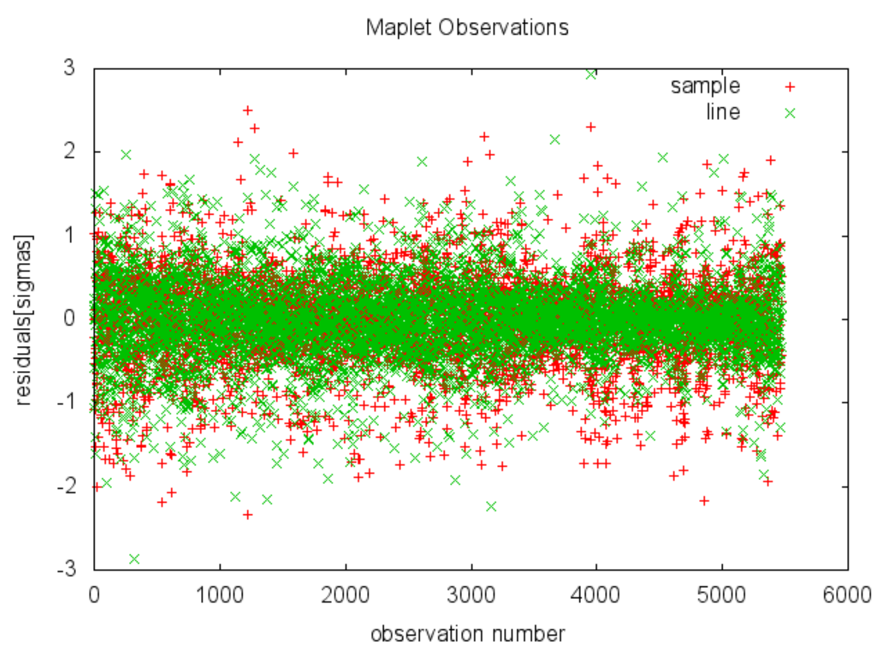

Figure 13. Bundle adjustment normalized residuals on landmark observations.

The rotational parameters of Lutetia can be estimated using only pure optical results and the nominal attitude commanded to Rosetta. The inertial attitude of the s/c and the attitude of the asteroid relative to the s/c are known therefore the inertial attitude of Lutetia was computed and used to fit a pure rotation. The obtained results were (1-σ uncertainties) a rotation period of 8.643 ±0.028 hours and spin axis right ascension and declination of 51.2 ±0.5 degrees and 11.0 ±0.7 degrees respectively, which is consistent with other published results. The result derived after the flyby by the Osiris science team was 51.8° +/- 0.4° in right ascension, and 10.8° +/- 0.4° in declination (see [10]). The spin axis orientation estimation obtained with maplet observations is in better agreement than the result obtained with manual observations in [2]

3.2 Orbit determination

The L-map observations were used in a full orbit determination solution combined with radiometric s/c tracking (2-way range and range-rate) plus directions from Rosetta to Lutetia centroid in the optical images taken from further distances (in which the apparent size of Lutetia was too small to identify landmarks).

The set of estimated parameters consisted of: Rosetta and Lutetia heliocentric orbits, Lutetia attitude state (spin axis orientation and rotation rate), Lutetia gravitational parameter (μ), landmark coordinates in asteroid-fixed frame, camera orientation correction per image (as rotations around the 3 camera axis), s/c acceleration calibrations (Solar radiation pressure, orbit correction maneuvers, wheel-of-loadings residual ΔV), and range biases per pass. The filter setup included also consider parameters for ground station coordinates, Earth Orientation parameters, tropospheric and ionospheric corrections.

The observation arc spanned from 2010/02/04 to 2010/07/17. A preliminary Rosetta solution was generated using only radiometric data up to the first Lutetia observation from the s/c (2010/05/31). The resulting estimated parameters and covariance were then used as a priori information for the OD runs using the rest of the observations arc around the flyby. Following plots show the OD post-fit residuals for the landmark observations based on L-maps.

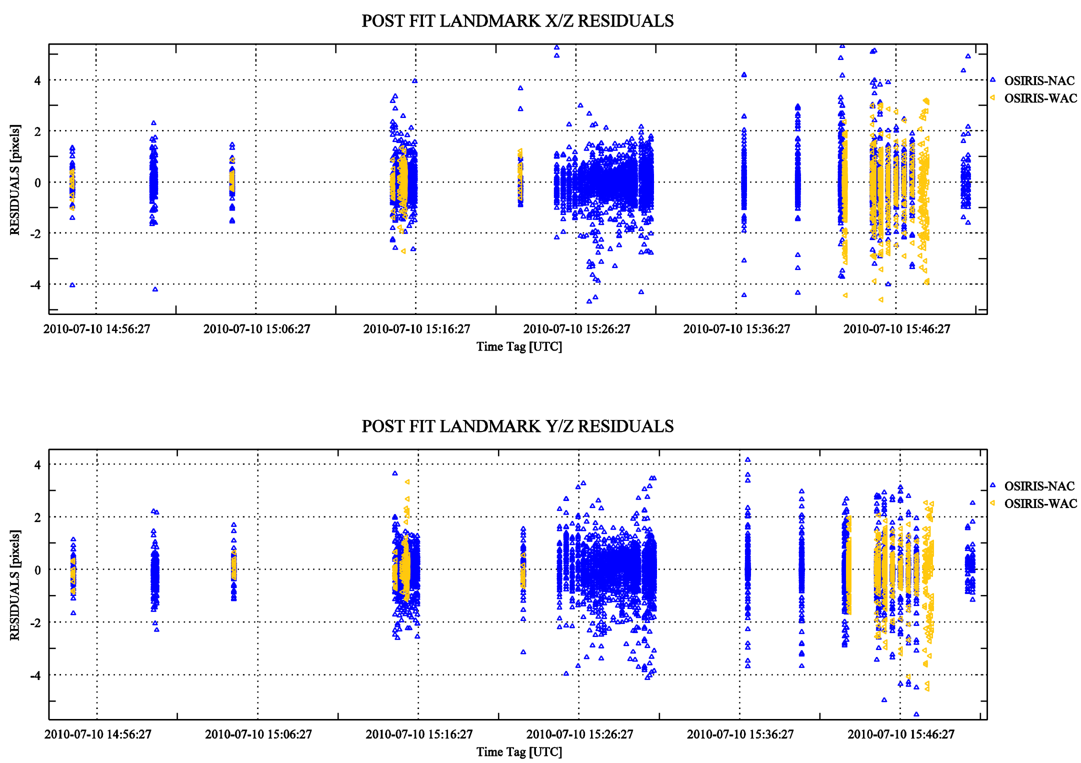

Figure 15. Post-fit landmark residuals evolution in time.

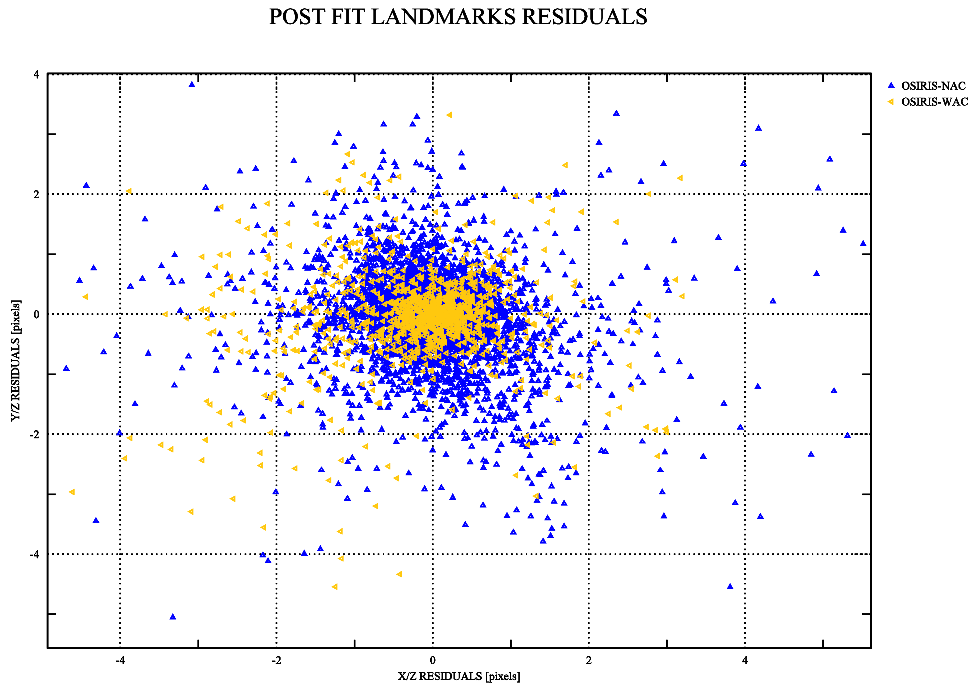

Figure 16. Post-fit landmark residuals in image plane.

The results of the OD show that the L-map observations are compatible with the other data types used in the OD, getting a solution close to the official trajectory reconstruction. The post-fit landmark residual statistics are very close to the ones obtained with the bundle-adjustment run: 0.75 (NAC) and 0.87 (WAC) pixels RMS for the L-map observations. Moreover, the obtained normalized residual RMS is close to 1, proving that the sigma value obtained from the correlation step is an accurate indicator of the observation quality.

As it was expected, the landmark observations did not add any information to the estimation of the flyby minimum distance or the Lutetia gravitational parameter. Due to the remaining uncertainty in the location of Lutetia's centre of mass in the landmark-fixed frame, only a small improvement in the formal covariance was obtained in the relative position along the flyby direction and in the direction perpendicular to the flyby plane. On the other hand, the use of L-map observations significantly reduced (by a factor of 2.5) the formal covariance of Lutetia spin axis orientation with respect to the manual landmarks case. This happened also with the rotation period of Lutetia when a very big a priori uncertainty was configured, so that the post-fit covariance showed the amount of information provided by the available observations. However, as it was already stated in [2], the post-fit uncertainty on the rotation period is orders of magnitude bigger than the current best estimate obtained by light-curve analysis based on observations from ground.

3.3 Shape reconstruction

A preliminary shape model was available from [2] that had been obtained with a silhouette and shadow carving method. Since L-maps where available on the observed part of Lutetia, this information was used to improve notably the surface characterization. Each vertex of the surface was projected onto the local available L-map and the albedos of the façades were also extracted.

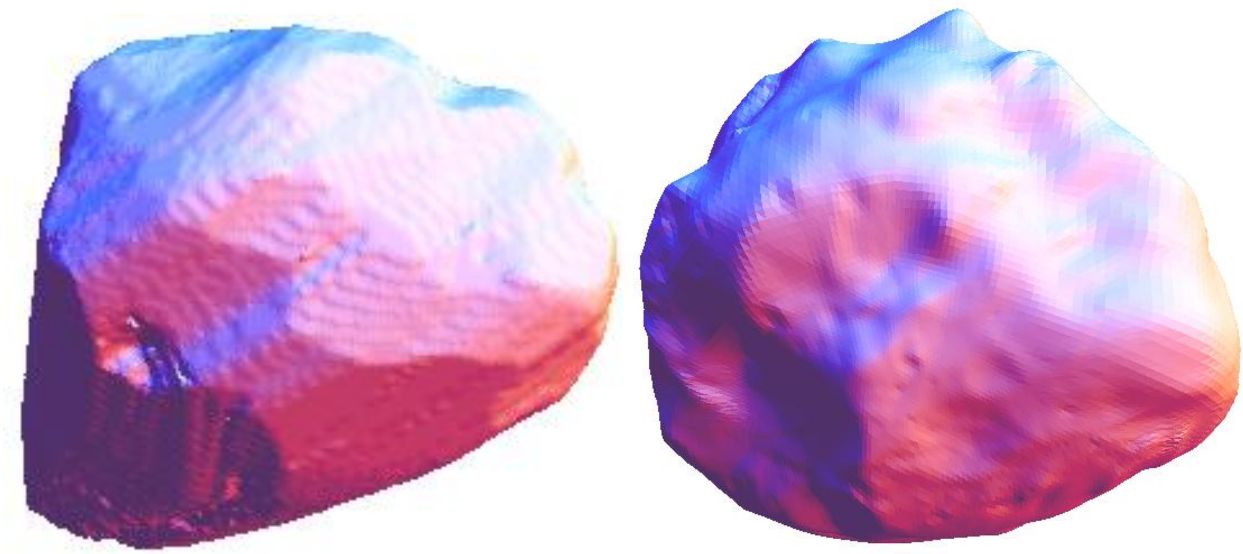

Figure 17. Lutetia preliminary shape (left) and final shape (right).

In Fig. 17, a 3D visualization is presented of asteroid Lutetia that was assembled from the set of L-maps with 0.5 km cell size. Using the smaller L-maps was not necessary because the initial shape had edges of ca. 1 km in length. Using L-maps of higher spatial resolution, a high-resolution shape model could be build. However this was not the intention of this work.

3.4 Image simulation

As mentioned in the introduction, image simulation software was implemented as support for optical navigation. Among other uses, such image simulator will also constitute an important tool to assess the quality of the L-maps technique. By comparing synthetic images with the correspondent real images downloaded from the S/C, it will in fact be possible to a posteriori evaluate the accuracy of the shape reconstruction and of the trajectory determination processes, implicitly validating the automatic landmarks observations with L-maps.

The image simulator has at its core a rendering engine which contains a photometric model very similar to that described in Section 2.1, which computes the signal on a given pixel starting from the geometry parameters of the body-sun-spacecraft system (α, d_S) and of the local surface (e, i), the constant photometric parameters (K_0, α_0, β_0), and the camera parameters (K_{CAM}, t_I, Φ). An efficient algorithm was developed to cope with large shape models (several million facets and vertices) in scanning the facets mapped to each pixel position. Subpixeling and shadowing calculations were also implemented, in order to smooth the rendered image and to deal with irregular body shapes. Finally, pixel convolution for Point Spread Function effects and a Gaussian photon noise were introduced as last steps of the image simulation process to further increase the synthetic images fidelity.

Rendering results of the L-map shape were compared with true images acquired by the Osiris NAC at the Lutetia fly-by. One image pair is shown in Fig 18 corresponding approximately to the closest approach. At this point, Lutetia appears larger than the NAC field of view, where the distance is only ~3300 km. The geometry of the fly-by is clearly well reconstructed, as is the overall limb and main features of the asteroid's shape.

Figure 18. NAC image approximately at closest approach (~3300 km). True image on the left, synthetic image from L-maps shape on the right.

4. Conclusions

An L-map methodology for identifying landmarks was presented with a technique that combines stereophotoclinometry and stereophotogrammetry to obtain landmark maps (L-maps).

This technique was applied to the Lutetia fly-by scenario. L-maps were generated all around the observed surface of the asteroid, and automatic landmark observations were obtained for all the available images acquired within a certain distance from Lutetia. The visible areas were reconstructed with a broader coverage and the quality of the automatic observations is higher with respect to the visually obtained ones. This improvement in the measurement accuracy was translated into a more precise orbit determination and asteroid dynamics estimation.

The L-maps were combined to assemble a medium-resolution shape model which represents a significantly better characterization of Lutetia with respect to the previous method that involved a silhouette carving technique (ISSFD2012). The shape recovery's accuracy was verified with the support of image simulation software.

This technique was developed in the frame of the Rosetta cometary phase and is intended to be gradually phased in the operations during the long comet-phase, in order to drastically relieve the operational workload, as well as to increase the landmark coverage of Churyumov-Gerasimenko and to improve the quality of the optical measurements.

5. References

[1] H. U. Keller et al., “OSIRIS the Scientific Camera System On-board Rosetta”, Space Science Reviews, Volume 128, Issue 1-4, pp. 433-506, 2007.

[2] M. Lauer, S. Kielbassa, R. Pardo de Santayana, “Optical measurements for attitude control and shape reconstruction at the Rosetta flyby of asteroid Lutetia” ISSFD2012 paper, International Symposium of Space Flight Dynamics, Pasadena, California, USA. 2012.

[3] F. Castellini, R. Pardo de Santayana, Wokes D., Kielbassa S., Optical Navigation For Rosetta Operations Near Comet Churyumov-Gerasimenko, Proceedings of 2013 AAS/ AIAA Astrodynamics Specialist Conference, Hilton Head, South Carolina, August 2013.

[4] J.-Y. Li et al, “Photometric analysis of 1 Ceres and surface mapping from HST observations” Icarus, Vol 182, pp. 143-160, 2006.

[5] R. W. Gaskell, “Landmark Navigation and target characterization in a simulated Itokawa encounter” Astrodynamics Specialists Conference , Lake Tahoe, California, USA, 2005.

[6] Scholten et al, ”Mars Express HRSC Data Processing Methods and Operational Aspects” Photogrammetric Engineering & Remote Sensing Vol. 71, No. 10, pp. 1143–1152, October 2005.

[7] C. C. Paige and M. A. Saunders, “LSQR: an algorithm for sparse linear equations and sparse least squares” ACM Transactions on Mathematical Software, Vol 8, No. 1, March 1982, pp. 43-71, 1982.

[8] R. W. Gaskell et al, “Characterizing and navigating small bodies with imaging data” Meteoritics and Planetary Science 43, Nr 6, 1049-1061, 2008.

[9] D. Wokes, J. Essert, “Development of Rosetta's Initial Stage Comet Rendezvous Guidance Systems”, AIAA GNC/AFM/MST/ASC, 2012.

[10] H. Sierks et al., “Images of Asteroid 21 Lutetia: A Remnant Planetesimal From the Early Solar System”, Science Volume 334, October 2011